Design of multi-bandwidth frequency selective surfaces for near infrared filtering

Thomas A. Cwik[a], Salvador Fernandez[b], A. Ksendzov[a], Clayton C. La Baw[a], Paul D. Maker[a], Richard E. Muller[a]

[a]Jet Propulsion Laboratory, California Institute of Technology, 4800 Oak Grove Dr., Pasadena, CA 91109
[b]Ciencia, Inc., 111 Roberts St., Suite C, East Hartford, CT 06108

ABSTRACT

This paper describes the design of infrared filters using methods drawn from microwave and millimeter wave filters. Special note is made of approximations made in the infrared design, and ways to improve upon these approximations. Results from the design, manufacture and test of linear wedge filters built using microlithographic techniques and used in spectral imaging applications will be presented.

Keywords: frequency selective surfaces, infrared filters, electromagnetic modeling, imaging spectroscopy, wedge filter

1. INTRODUCTION

Frequency selective surfaces are widely used in the microwave and millimeter wave regions of the spectrum for filtering signals. They are used in telecommunication systems for multi-frequency operation or in instrument detectors for spectroscopy. The frequency selective surface operation depends on a periodic array of elements resonating at prescribed wavelengths producing a filter response. The size of the elements is on the order of half the electrical wavelength, and the array period is typically less than a wavelength for efficient operation. When operating in the optical region, diffraction gratings are used for filtering. In this regime the period of the grating may be several wavelengths producing multiple orders of light in reflection or transmission.

In regions between these bands (specifically in the infrared band) frequency selective filters consisting of patterned metal layers fabricated using electron beam lithography are beginning to be developed. The operation is completely analogous to surfaces made in the microwave and millimeter wave region except for the choice of materials used and the fabrication process. In addition, the lithography process allows an

arbitrary distribution of patterns corresponding to resonances at various wavelengths to be produced.

The design of sub-millimeter filters follows the design methods used in the microwave region. Exacting modal matching, integral equation or finite element methods can be used for design. A major difference though is the introduction of material parameters and thickness' that may not be important in longer wavelength designs. This paper will describe the design of infrared filters using methods drawn from microwave and millimeter wave filters. Special note will be made of approximations made in the infrared design, and ways to improve upon approximations. Results from the design, manufacture and test of linear wedge filters built using microlithographic techniques and used in spectral imaging applications will be presented.

2. DESIGN OF MULTI-BANDWIDTH INFRARED FILTER ARRAYS

A multi-bandwidth infrared filter array consists of an array element within a two-dimensional periodic cell. The filter bandwidth, center frequency and polarization properties are dependent upon the shape and size of this element. Different element shapes are used for different applications depending on the design specification. To model a single layer frequency selective surface, a calculation for the induced current on the metallic periodic array deposited on a layered substrate is performed. To model the multiple layering of the design, the scattering parameters due to each screen are cascaded in a separate calculation. The frequency selective surface analysis uses sub-domain basis functions to model the current in a periodic cell. An overview of the analysis is now developed[1].

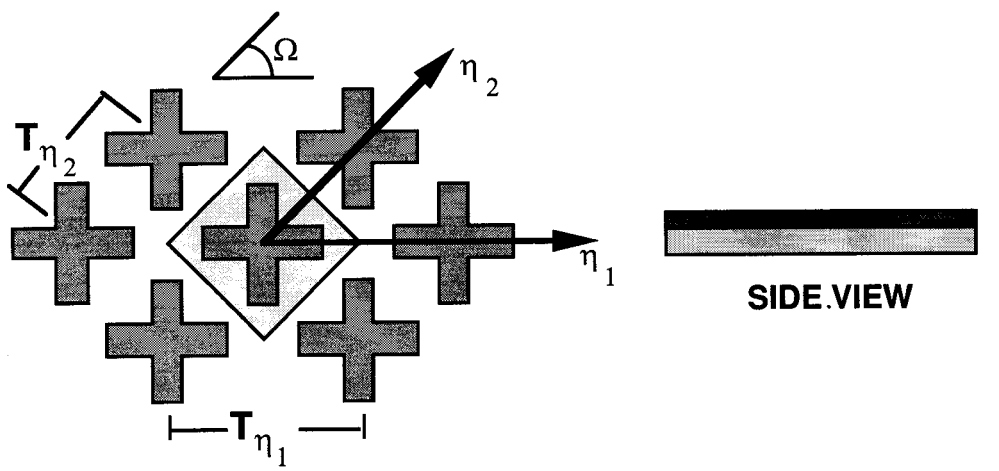

Figure 1. Geometry of crossed-slot frequency selective surface.

2.1 Single layer frequency selective surface analysis

The geometry of a crossed slot periodic surface is shown in Fig. 1. Periodicities are T_{η_1} and T_{η_2} in the non-orthogonal (η_1, η_2) coordinate system. Multiple dielectric layers are included below and above the metal slot array. The scattered electric field in all space due to an induced current may be found from the source-field relationship

$$\bar{E}^s(\bar{\rho},z) = \frac{1}{j\omega\varepsilon}(\nabla\nabla + k^2\mathbf{I})\cdot\bar{A}(\bar{\rho},z) \tag{1}$$

where the vector potential is

$$\bar{A}(\bar{\rho},z) = \int_{-\infty}^{+\infty}\bar{J}(\bar{\rho}',z)\frac{e^{-jkR}}{4\pi R}d\bar{\rho}' \tag{2}$$

and the distance R is $[(x-x')^2+(y-y')^2+z^2]^{1/2}$ (The current lies in the plane z' = 0 without loss of generality.) Consistent with Floquet's condition, the support of the current may be reduced from that existing over the entire plane z' = 0 to that of one cell, i.e.,

$$\bar{J}(\bar{\rho}) = \sum_{mn=-\infty}^{\infty}\tilde{\bar{J}}_{mn}\Psi_{mn}(\bar{\rho}) \tag{3a}$$

where

$$\tilde{\bar{J}}_{mn} = \int_{\partial S}\bar{J}(\bar{\rho}')\Psi^*_{mn}(\rho')d\bar{\rho}' \tag{3b}$$

and where the transverse component of the m,nth Floquet harmonic is

$$\Psi_{mn}(\bar{\rho}) = \frac{1}{(T_xT_y)^{1/2}}e^{j\bar{k}_{mn}\cdot\bar{\rho}} \tag{4}$$

The associated propagation constant is

$$\bar{k}_{mn} = \hat{x}k_{x_m} + \hat{y}k_{y_n} \tag{5}$$

where

$$k_{x_m} = \frac{2\pi}{T_x}m + k_{x_0} \tag{6a}$$

$$k_{y_n} = \frac{2\pi}{T_y}n + k_{y_0} \tag{6b}$$

The z component of the propagation vector is

$$k_{z_{mn}} = (k^2 - k_{x_m}^2 - k_{y_n}^2)^{1/2} \tag{7}$$

and the negative imaginary branch is taken when $k_{x_m}^2 + k_{y_n}^2 > k^2$.

Equation (3) defines a transform pair and is recognized as the Fourier series representation of the induced current multiplied by the phase of the incident field. A direct construction of the scattered field in terms of the Floquet harmonics involves the transform of the free-space Green's function.

$$\frac{e^{-jkR}}{4\pi R} = \frac{1}{(2\pi)^2}\int_{-\infty}^{\infty} \frac{e^{-jk_z|z|}}{2jk_z} e^{j\bar{k}\cdot(\bar{\rho}-\bar{\rho}')}\, d\bar{k} \tag{8}$$

where the propagation vector is continuous. Substituting the Floquet representation of the current (3a) along with the Fourier representation of the Green's function into the potential results in

$$\bar{A}(\rho,z) = \sum_{mn=-\infty}^{\infty} \tilde{\bar{J}}_{mn} \frac{e^{-jk_{z_{mn}}|z|}}{2jk_{z_{mn}}} \Psi_{mn}(\bar{\rho}) \tag{9}$$

Summations and integrations have been interchanged, and use has been made of the transform pair

$$\frac{1}{(2\pi)^2}\int_{-\infty}^{\infty} e^{j(\bar{k}_{mn}-\bar{k})\cdot\bar{\rho}}\, d\bar{\rho} = \delta(\bar{k}_{mn} - \bar{k}) \tag{10}$$

Completing the indicated differentiations of (1) results in the representation of the scattered electric field

$$\bar{E}^s(\rho,z) = \frac{1}{j\omega\varepsilon}\sum_{mn}\frac{1}{2jk_{z_{mn}}}\begin{bmatrix} k^2 - k_{x_m}^2 & -k_{x_m}k_{y_n} \\ -k_{x_m}k_{y_n} & k^2 - k_{y_n}^2 \end{bmatrix} \cdot \tilde{\bar{J}}_{mn}\Psi_{mn}(\bar{\rho})e^{-jk_{z_{mn}}|z|}$$

$$= \frac{1}{j\omega\varepsilon}\sum_{mn} Z_{mn}\cdot\tilde{\bar{J}}_{mn}\Psi_{mn}(\bar{\rho})e^{-jk_{z_{mn}}|z|} \tag{11}$$

The scattered magnetic field may be similarly found from the relation

$$\bar{H}^s(\bar{\rho},z) = \nabla\times\bar{A}(\bar{\rho},z) \tag{12}$$

2.2 The impedance boundary condition

To account for losses in the metallic material, an impedance boundary condition is used. A rigorous examination of non-perfectly conducting surfaces would require the calculation of induced volume currents in the lossy material. (The metallic region would have an electrical thickness dependent upon material parameters and wavelength.) The surface impedance boundary condition allows the volume formulation to be approximated by an analysis considering only the surface current and is written as

$$\bar{E}^i + \bar{E}^s = R\bar{J} \tag{13}$$

where tangential fields are implied and the equation holds over the support of the current. The complex impedance R depends upon the material parameters and electrical thickness of the metal. For metallic materials which greatly attenuate the field as it penetrates the medium, R is the medium impedance $\sqrt{\mu/\varepsilon}$ where ε is the complex permittivity of the medium. Conversely, for materials which allow little attenuation and phase shift of the field as it penetrates the medium, R is $\sqrt{\mu/\varepsilon}/kt$ where k is the complex propagation constant of the material and t is the thickness of the patch. With the scattered field given by (11), the impedance boundary condition is written as

$$R\bar{J} - \frac{1}{j\omega\varepsilon}\sum_{mn} Z_{mn}\cdot\tilde{\bar{J}}_{mn}\Psi_{mn} = \bar{E}^i \tag{14}$$

where tangential components in the z = 0 plane are implied. For materials in the infrared, measurements give the loss factors for metals used, and indicate that the first approximation above is to be applied. This approximation can be improved by using volumetric techniques such as a finite element method to calculate fields in the lossy materials.

2.3 Sub-domain expansion functions

Equation (14) is the unique relation for the induced current with its solution yielding the reflection and transmission coefficients of the structure. To model an arbitrary size crossed-slot or other shape within the periodic cell, sub-domain rooftop basis functions are chosen to represent the current. This is especially important in patterned arrays that do not conform to standard shapes as in microwave design. These functions model the current distribution and allow the scattered field to be given by a convergent series. As seen in Fig. 2, the current approaches zero in the direction of flow at the patch edges and is nonzero in the direction of flow parallel to the edges allowing for the representation of the edge singularity. Each subsection of current extends over two patches of the grid, longer in the direction of the current, with at least one x directed and y-directed rooftop overlaying each patch. The subsection is sampled at the center of each rooftop.

As shown in Fig. 2, the sample points of each subsection of current are shifted from the center point of its associated patch. A coordinate system is chosen such that the sample points of the grid lie at the center of each patch. The sample points of the rooftops representing the y component of the current are then shifted to the edge of the patch in the positive x direction, and similarly, the sample points of the rooftop representing the y component of the current are shifted to the edge of the patch in the positive y direction.

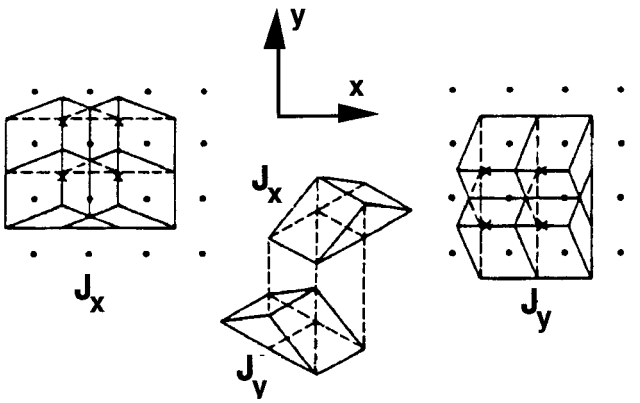

Figure 2. Diagram of rooftop sub-domain basis functions used to represent current.

2.4 Cascade connection of scattering parameters

To model the multiple layers of the frequency selective surface, scattering parameters of each single FSS layer are calculated and cascaded[2]. The single layer frequency selective surface consists of the metallic array and any number of other dielectric layers that may exist. The scattering parameters for this sandwich structure are calculated and then combined with those of other layers of possible different element sizes. A composite scattering matrix

$$\begin{bmatrix} \overline{V}^{\alpha_s} \\ \overline{V}^{\gamma_s} \end{bmatrix} = \begin{bmatrix} \mathbf{S}^{\Sigma}_{\alpha\alpha} & \mathbf{S}^{\Sigma}_{\alpha\gamma} \\ \mathbf{S}^{\Sigma}_{\gamma\alpha} & \mathbf{S}^{\Sigma}_{\gamma\gamma} \end{bmatrix} \cdot \begin{bmatrix} \overline{V}^{\alpha_i} \\ \overline{V}^{\gamma_i} \end{bmatrix} \tag{15}$$

is computed which contains the transmission and reflection coefficients of the entire frequency selective surface.

3. MANUFACTURE OF A LINEAR VARIABLE FILTER ARRAY

Linear Variable Filters (LVF's or "wedge filters") have found increasing applicability in spectrally selective optical instruments. They serve as moderate resolution spectral discriminators in astronomical instruments and in reconnaissance equipment. They perform extremely well as "sliding out-of-band blocking filters" when used in conjunction with grating spectrometers[3]. Visible band LVF's fabricated using traditional interference filter technology have become available and form the basis of a

number of spectral imager and imaging spectrometer designs. The desire to extend the instrumentation into the infrared region has been often stated. Additionally, commercial providers of devices using LVF's desire readily available parts and consistent specification. An earlier discussion on these applications and our design has been outlined[4].

We have manufactured wedge filters covering the 2.5 - 5μm spectral range by patterning thin metal films using the electron beam lithography technique. Arrays of apertures with varying size and pitch were manufactured in a gold layer deposited on a calcium fluoride substrate. This technique can produce large area arrays (up to 1.5 cm × 1.5 cm), offers high reproducibility and allows arbitrary tailoring of the bandpass wavelength versus position profile, unlike dielectric layer interference wedge filters that offer linear grading only. The opportunity to specify a particular wavelength versus position sequence to emphasize certain spectral regions is very attractive to both commercial and government agency users.

In the past, near infrared mesh filters have been successfully manufactured by electron-beam lithography by Byrne *et al*[5]. This group manufactured patterns using direct-write electron beam (e-beam) lithography on PMMA. More recently, focused ion beam (FIB) lithography process have been developed for producing frequency selective metal mesh patterns[6,7].

While both direct write on PMMA and FIB techniques enable patterns with fine line features (better than 200 nm), they are not suitable for wedge filter manufacture. The FIB technique involves stepping of a mask and therefore can not produce patterns of elements with varying pitch without stitching discontinuities. The use of PMMA would lead to prohibitively long writing times for the pattern sizes required to cover a typical wedge filter area. Since our writing time can not exceed 64 hrs., the filter area would be limited to 6-7 mm^2. We have adopted a processing sequence similar to the one described by Atkinson et al[8]. We utilized Shipley 601 negative e-beam resist which reduces the required exposure and, consequently, the writing time approximately 40-fold. This allows us to write arrays as large as 250 mm^2.

In brief, the processing sequence is as follows. First, a layer of PMMA was spun on the CaF_2 substrate. The layer was cured at 170°C and then covered with 100 A of Ge via thermal evaporation. The e-beam resist (Shipley-601) was spun over the Ge layer, cured and exposed. The developed resist served as a mask for patterning the Ge layer by the reactive ion etching (RIE) using CF_4. Then the PMMA was patterned in low pressure oxygen RIE using the Ge layer as a mask. These processing steps transferred the written pattern onto the PMMA layer that was used for a metal lift-off. The metal was 800 A gold layer with 60 A Cr strike layer. The electron micrograph of a sample before metal deposition is shown in Fig. 3. A micrograph of a completed mesh filter is shown in Fig. 4.

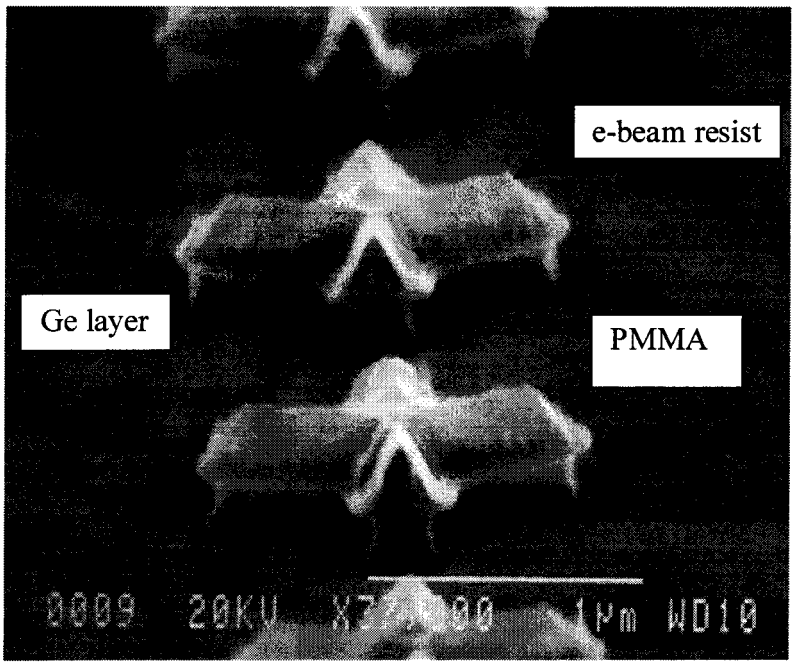

Figure 3. Micrograph of intermediate process step

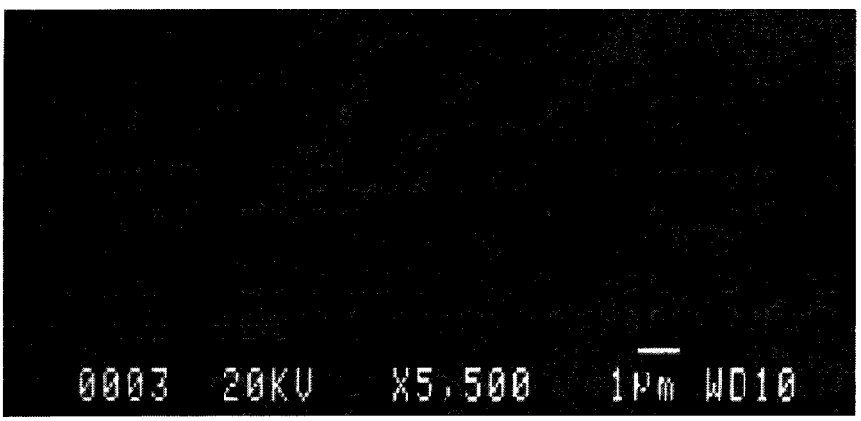

Figure 4. Mesh filter micrograph

4. TEST RESULTS

We have produced and measured a wide area (1 cm^2) single wavelength filter. In Figure 5 we present the comparison of the calculated and measured transmittance curves. The measurements were performed using a Beckman IR4250 Spectrophotometer in an f/10 beam. The calculated and measured curves agree well. The filter has very good rejection at wavelengths longer than the center of the pass band. There is an undesirable

transmission band on the shorter wavelength side that turned out to be somewhat larger than predicted. The main transmittance peak parameters are summarized in Table 1

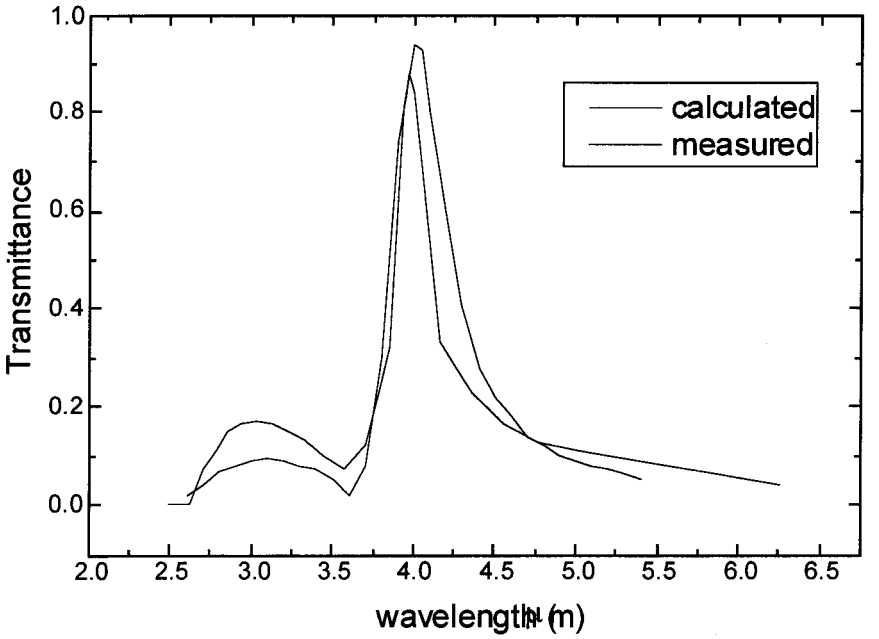

Figure 5. Calculated and measured single filter transmittance.

Table 1. Single filter bandpass characteristics.

	T_{max}	λ_{max} (μm)	$\Delta\lambda$ (μm) FWHM
Calculated	0.95	4.00	0.40
Measured	0.88	3.97	0.28

The filters described above can be manufactured as spatially wavelength variant by varying the geometry (spacing and scale of the array elements). One such filter has been fabricated and tested in the Beckman IR 4250 Spectrophotometer using the JPL Micro Scale Test Adjunct[9]. To facilitate testing, the filter has been implemented as a series of eleven one-millimeter wide constant wavelength stripes. The transmittance *vs.* position on the filter is shown in Figure 6a for three of the stripes. The predicted and measured spectral positions of the passbands are in good agreement as shown in Figure 6b.

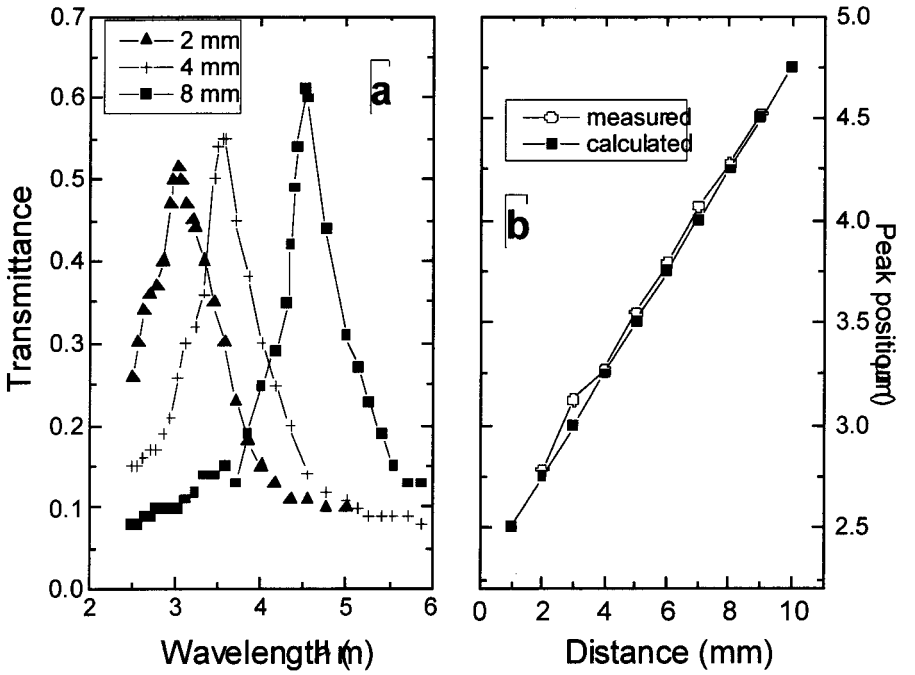

Figure 6. Variable filter transmittance vs. distance from the filter edge.

5. CONCLUSIONS

We have demonstrated accurate design of wedge filters using metal grids in 2.5-5μm range. From methods used in the microwave and millimeter-wave regions of the spectrum, we have developed models that accurately predict the center resonance of the filter. The filter bandwidth is not as accurately predicted, perhaps due to the approximations used in modeling the lossy infrared materials. Additional accuracy may be found using volumetric finite element methods to model the materials and specific shapes encountered in infrared design.

6. ACKNOWLEDGMENT

The research described in this paper was carried out by the Jet Propulsion Laboratory, California Institute of Technology, under contract with the National Aeronautics and Space Administration. Sponsorship of this research lies with the Department of Defense Ballistic Missile Defense Organization under the auspices of a Small Business Technology Transfer Program managed by Ciencia, Incorporated of East Hartford, CT.

7. REFERENCES

1. Cwik T. and Mittra R., "Scattering from a periodic array of free-standing arbitrarily shaped perfectly conducting or resistive patches", *IEEE Trans. Antennas Propag.*, vol. AP-35, no. 11, pp. 1226-1233, Nov. 1987.

2. Cwik T. and Mittra R, "The cascade connection of planar periodic surfaces and lossy dielectric layers to form an arbitrary periodic screen", *IEEE Trans. Antennas Propag.*, vol. AP-35, no. 12, pp. 1397–1405, Dec. 1987

3. La Baw, C. "Thermal Infrared Imaging Spectrometry with Room Temperature Optics", *Proc. Intl. Symposium on Spectral Sensing Research*, 1993 and *Proc. SPIE OE/LASE '93*, vol. 1874, No. 29, 1993

4. Ksendzov, A., Fernandez, S., Cwik, T., La Baw, C. Maker, P. and Muller R., "Wedge Filters for Spectral Imaging in the Near IR Using Metal Grids, *Proceedings Infrared Astronomical Instrumentation. Vol 3354*, 1998.

5. D. M. Byrne, A.J. Brouns, F.C. Case, R.C. Tiberio, B.L. Whitehead, and E.D. Wolf. "Infrared mesh filters fabricated by electron-beam lithography", *J. Vac. Sci. Technol.* B 3 (1) pp. 268-271 (1985).

6. J.C. Wolfe, S.V. Pendharkar, P. Ruchhoeft, S. Sen, M.D. Morgan, W.E. Horne, R.C. Tiberio, and J.N. Randall. "A proximity ion beam lithography process for high density nanostructures", *J. Vac. Sci. Technol.* B 14 (6) 3896-3899 (1996).

7. M.D. Morgan, W.E. Horne, V. Sundaram, J.C. Wolfe, S.V. Pendhakar, R. Tiberio. "Application of optical filters fabricated by masked ion beam lithography", *J. Vac. Sci. Technol.* B 14 (6) 3903-3906 (1996).

8 G.M. Atkinson, R.L. Kubena, L.E. Larson, L.D. Ngyen, F.P. Stratton, L.M. Jelloian, M.V. Le, and H. McNulty. "Self-aligned high electron mobility transistor gate fabrication using focused ion beams", *J. Vac. Sci. Technol.* B 9 (6) 3506-3510 (1991)

9. La Baw, C. "Measuring Spatially Varying Transmittance of a Filter", *NASA Tech Briefs*, pg. 66, September 1992